JOURNAL OF APPLIED ELECTROCHEMISTRY 4 (1974) 155–161

# *Transpassive dissolution of mild steel in $NaNO_3$ electrolytes*

D-T. CHIN and K-W. MAO

*Electrochemistry Department, Research Laboratories, General Motors Corporation, Warren, Michigan, U.S.A.*

Received 22 August 1973; revised MS received 7 November 1973

A study has been made of the transpassive dissolution of mild steel in sodium nitrate solution over a range of current densities from 2 to 100 A $cm^{-2}$. The dissolution current efficiency and the anode potential free from the electrolyte IR component were measured in a flow cell; optical and scanning electron microscopy were then used to examine the sample surfaces after the dissolution tests. The results show that during the early stage of transpassive dissolution, the mild steel is covered with a compact, electronically conductive $Fe_3O_4$ film, and the current is consumed mainly in oxygen generation on the film/electrolyte interface. With increasing anode potential and current density, this film is gradually broken and the underlying metal surface becomes exposed to the electrolyte. At this stage, iron dissolution begins at a high rate. The film rupturing process is strongly dependent on nitrate concentration; the higher this is, the lower is the current density required to rupture the film.

## 1. Introduction

It has been found in previous studies [1, 2] that dimensional control in electrochemical machining (ECM) is quantitatively related to the current efficiency for metal removal. For a given anode geometry, the current density is highest at the machining area directly facing the cathode. At other sites on the anode, the current density decreases asymptotically to zero with increasing distance from the machining area. During the ECM of steel in NaCl electrolytes, metal is removed at 100% current efficiency, and the current efficiency is nearly independent of the current densities over the anode surface; thus undesired stray cutting takes place at sites located some distance from the machining area. In $NaNO_3$ and $NaClO_3$ electrolytes, the current efficiency is found to decrease with decreasing anodic current density. This gives rise to highly localized metal removal on the machining area, and good dimensional control can be achieved in these electrolytes.

As the same variation in dissolution current efficiency dependence on current density has been found during the electrochemical machining (ECM) of nickel and copper alloys [2, 3], understanding the cause would be of theoretical interest and practical importance to the further development of the ECM process. A series of studies are reported of the mechanism of transpassive dissolution of mild steel in $NaNO_3$ electrolyte. The dissolution current efficiency and the anode potential free from the electrolyte IR component were measured in a flow cell at controlled anodic current densities ranging from 2 to 100 A $cm^{-2}$. Optical and scanning electron microscopy were used to examine the sample surfaces after the dissolution tests.

It has been found [4] that mild steel begins to be passivated at a potential of 0 V versus SCE in neutral nitrate solutions and that the transition from passive to transpassive dissolution occurs at a potential of approximately 1·2 V versus SCE. The passivation is initiated by the spreading of a monolayer of oxide film on the anode surface. The ECM is presumably taking place at transpassive potentials. Since low dissolution

current efficiency is always obtained during the ECM of steel in nitrate solutions at moderately high current densities (10 A $cm^{-2}$), it was suggested that this oxide film was a good electronic conductor which continued to exist even in the transpassive region of the polarization curve [5]. This hypothesis is confirmed by the results of the present study. It will be shown that during the early stage of the transpassive dissolution, the mild steel surface is covered with an electronically conductive $Fe_3O_4$ film and that the current is consumed mainly in the generation of oxygen at the film/electrolyte interface. With increasing anode potential and current density, the film is gradually broken due to intergranular attack caused by adsorbed anions. Once the oxide film is dislocated, the metal surface exposed to the electrolyte begins to dissolve at a high rate, resulting in an increase in the current efficiency.

## 2. Experimental

### *2.1 Anodic current efficiency measurement*

The flow cell system used for current efficiency measurements was described previously [1]. It consisted of an acrylic cell block, a 2-litre solution reservoir, a variable speed micro-pump and a rotameter. The flow channel in the cell block was 0·635 cm wide and 5·7 cm long in the flow direction. The cathode and the anode were located midway on the channel wall, and an initial electrode spacing of 0·04 cm was used for all measurements. The anode was a mild steel rod,* 0·318 cm in diameter. The cylindrical surface was insulated by the cell block; only the rod end, with a surface area of 0·0792 $cm^2$, was exposed to the electrolyte. The copper cathode was located opposite the anode and had a surface area of 0·4 $cm^2$ exposed to the flow channel. A capillary in the cell block with its tip flush with the anode plane was used to measure the anode potential.

Before each measurement, the end of the mild steel rod was polished with Carbimet 320-grit grinding paper, rinsed with water, and dried with a heat gun. The electrode was then weighed and installed in the flow channel. A constant current (Magna 4700 potentiostat) was then applied to the cell, and an Eagle Signal Flexopulse timer was used to control the dissolution time. The dissolution time varied from 5 s at 100 A $cm^2$ to 120 s at 2 A $cm^{-2}$. The anode potential versus SCE was recorded on a Sanborn 296 recorder. After dissolution, the steel rod was rinsed, dried and reweighed to determine the amount of metal removed. The current efficiency was calculated on the basis of ferrous ion as the dissolution product. The electrolytes used were 1–4 M $NaNO_3$, with pH values from 4 to 10. The pH was controlled by adding $HNO_3$ or NaOH to the solution reservoir during the run. The electrolyte flow velocity was kept at 1000 cm $s^{-1}$ in the flow channel; this corresponds to a Reynolds number of approximately 7000. All runs were made at 21 ± 1°C.

### *2.2 IR-free polarization measurements*

These were measured in a second flow cell using a current interruption method. A detailed description has been given elsewhere [6]. Briefly, the flow cell consisted of a flow channel with rectangular cross section, a brass cathode, a mild steel anode and a capillary to measure the anode potentials. The anode was 0·0635 cm wide by 0·254 cm long, with its short dimension parallel to the direction of flow. The cathode had the same dimensions as the anode and was placed opposite the anode in the flow channel. The initial distance between the anode and the cathode was 0·051 cm.

For each run, the anode surface was polished with 600-grit wet grinding paper and treated with 6 N HCl for 30 s followed by rinsing in water. The clean electrode was immediately transferred to the flow cell and a constant current, controlled by a Sorensen DCR 150–5A D.C. power supply, was applied. The anode potential versus SCE and the cell current were displayed on a Tektronix 555 dual-beam oscilloscope. After the anode potential had reached a steady state (which normally took less than 0·5 s), the current was interrupted with a mercury relay. The changes in the anode potential and the cell current were then recorded photographically

* Composition: Fe, 98·5%; C, 0·08%; S, 0·26%; P, 0·021%; Mn, 1·06%; Si, 0·004% Co, 0·02%; Ni, 0·05%

from an oscilloscope using a time scale of 20 $\mu$s cm$^{-1}$. To determine the IR-free potential of the anode, the oscillogram was enlarged 10 times under a microscope, and the IR portion of the anode potential obtained by a linear extrapolation of the anodic potential decay curve to zero time. In this way, IR-free polarization values were obtained for the dissolution of mild steel in 2–4 M $NaNO_3$ electrolytes over a range of current densities from 2·5 A cm$^{-2}$ to 100 A cm$^{-2}$ at a constant temperature of 26±2°C. The electrolyte flow velocity was varied from 500–2000 cm s$^{-1}$, corresponding to a range of Reynolds numbers from 4000 to 20 000 based upon the equivalent diameter of the flow channel.

## 3. Results

### *3.1 Current efficiency*

The current efficiency for the dissolution of mild steel in $NaNO_3$ as a function of current density is shown in Fig. 1 for three different nitrate

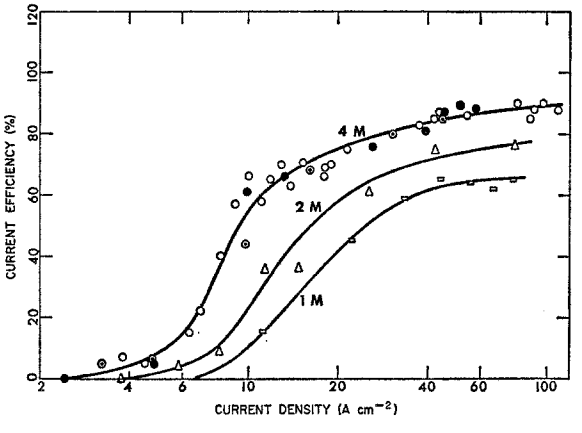


Fig. 1. Current efficiency for the dissolution of mild steel in $NaNO_3$ solutions on the basis of ferrous ion as the dissolution product. The pH of the solutions used was: ●—4·5; ○, △, □—6·5; and ⊙—10·3. These results were obtained at a Reynolds number of 7000; changes in the rate of electrolyte flow had no significant effect on the results.

concentrations. The curve for 4M $NaNO_3$ includes measurements at three different pH values ranging from 4·5 to 10·3, and the curves for 1 M and 2 M nitrate solutions were obtained at a pH of 6·5. Since the rate of electrolyte flow was found to have no effect on the results for flow beyond the choking limit [1], all the data reported were obtained at a Reynolds number of 7000 based upon the equivalent diameter of the flow channel. It is seen that the dissolution efficiency is an increasing function of anodic current density as well as nitrate concentration. Change in the pH of the electrolyte apparently has no significant effect on the current efficiency.

### *3.2 IR-free polarization curves*

Fig. 2 shows the results of IR-free polarization measurements in 2 M and 4 M $NaNO_3$ obtained

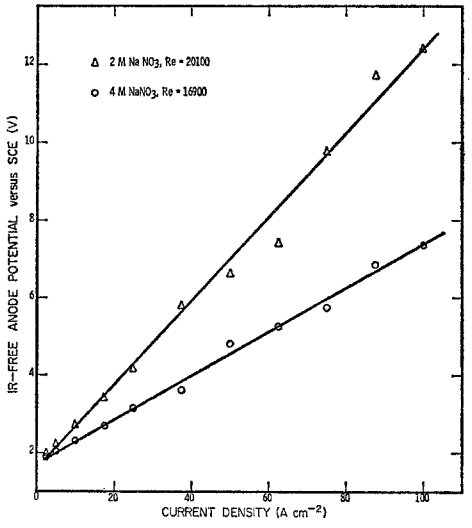


Fig. 2. Anodic polarization curves free from the IR-component contributed by the electrolyte between the reference capillary and the anode surface. *Re* is the Reynolds number based on the equivalent diameter of the flow cell.

at a flow velocity of 2000 cm s$^{-1}$. The corresponding Reynolds numbers are indicated in the figure. No significant difference was found in the results obtained at a lower flow velocity of 500 cm s$^{-1}$, although there was a tendency in the 2 M $NaNO_3$ for the anode potential to be slightly lower at the lower flow rate. Each point in the figure is an average of at least two runs. The reproducibility of the measurements was about 5%. Fig. 2 shows that the IR-free anode potential is a linear function of the anodic current density and not the usual logarithmic, Tafel relation. It might be thought that the deviation is due to incomplete IR compensation caused by an artifact in the experiment. That this is not an

artefact is shown in Fig. 3, where the IR drop in the electrolyte between the reference capillary and the anode is plotted against the anodic current density for 2–4 M $NaNO_3$ and 4 M NaCl[6]. The slope of these straight lines represents an apparent electrolyte resistance between the reference capillary and the anode [7]. The ratio between any two of the apparent resistances can be compared with the corresponding resistivity ratio reported in the literature. The results given in Fig. 3 indicate that, slope (2 M

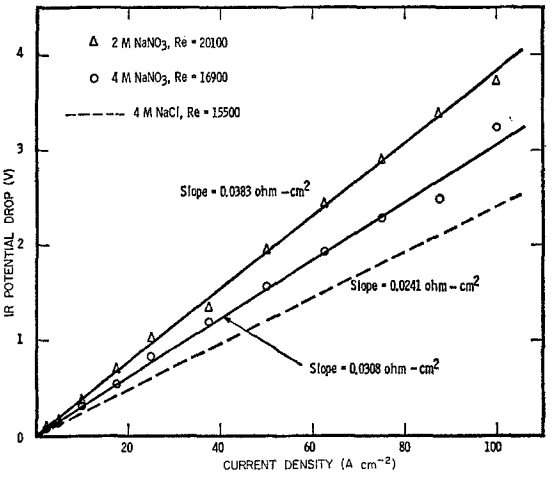


Fig. 3. IR drop between the reference capillary and the anode surface as a function of current density.

$NaNO_3$)/slope (4 M $NaNO_3$) = 1·24, and slope (4M $NaNO_3$)/slope (4M NaCl) = 1·28. The corresponding resistivity ratios given in [8] are 1·44 and 1·27; the agreement between the two sets of values is apparent. Thus, one may say with confidence that the potential values reported in Fig. 2 are free of the IR drop in the electrolyte.

### *3.3 Decay of open circuit potential*

A series of open-circuit potential decay curves are given in Fig. 4 for the dissolution of mild steel in 4 M $NaNO_3$. These curves were obtained on a recorder after disconnecting the current in the current efficiency experiment, the pH of the electrolyte being maintained at 9 throughout. The dissolution current density varied from 1·7 A $cm^{-2}$ for curve 4A to 16·2 A $cm^{-2}$ for curve 4E. Two potential arrests, equivalent to one

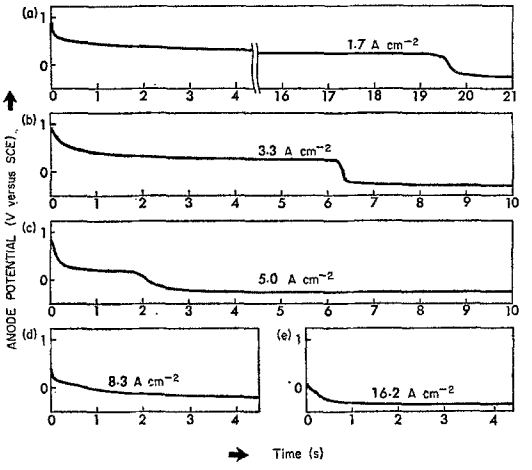


Fig. 4. Decay of open-circuit potentials after dissolution at various current densities in 4 M $NaNO_3$. The pH of the electrolyte was maintained at 9.

wave, can be observed on curves 4A-C. The point of inflection of the first arrest occurs at 0·5–0·75 V versus SCE and of the second at approximately 0 mV versus SCE. The first arrest potential corresponds to the reduction of $Fe_3O_4$ to FeO and $Fe^{++}$ [9], and the second to the active–passive transition potential reported earlier [4]. The length of the wave plateau appears to decrease with increasing current density. At 8·3 A $cm^{-2}$, the wave plateau has almost disappeared (Curve 4D). At 16·2 A $cm^{-2}$, only the second arrest is observed, and the anode potential drops to the open-circuit equilibrium value immediately after switching off the current (curve 4E).

Fig. 5 shows open-circuit potential decay curves in 4 M $NaNO_3$ at a faster time scale of 20 $\mu$s $cm^{-1}$. Fig. 5a was obtained at a current density of 10 A $cm^{-2}$, and Fig. 5b, at 75 A $cm^{-2}$. These are typical potential traces recorded on an oscilloscope during the current interruption experiment. After switching off the current, the anode potential immediately drops from a constant value to an arrest potential at approximately 1·6 V versus SCE and then to a steady value of 1·2 V versus SCE (Fig. 5b) corresponding to the oxygen evolution (or the passive–transpassive transition) potential for mild steel in nitrate solutions [4]. This phenomenon happened from 2·5 A $cm^{-2}$ to 100 A $cm^{-2}$ implying that oxygen was generated within this

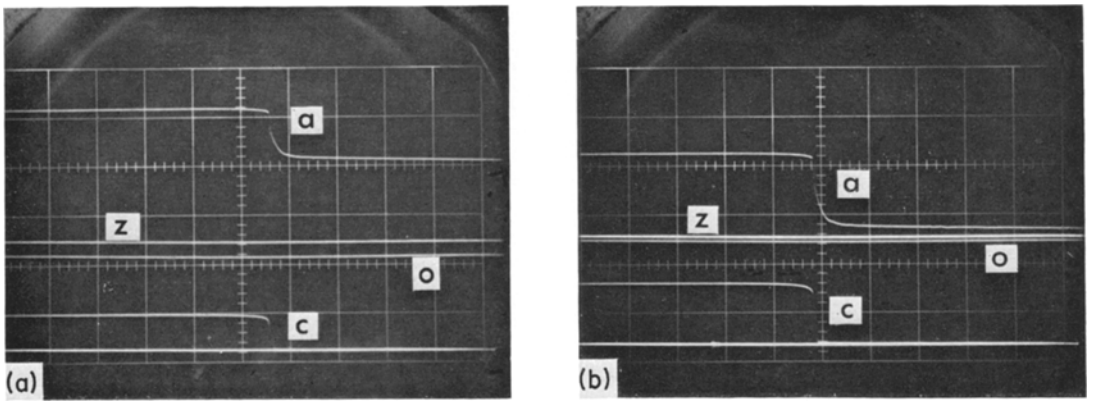


Fig. 5. Typical open-circuit decay curves in 4 M $NaNO_3$ at a faster time scale of 20 $\mu$s per div. Trace a is the anode potential at 1 V per div for part (a) and 5 V per div for part (b); trace c is the cell current; trace o is the open circuit equilibrium potential; and trace z is the zero point. The dissolution current densities before switching off the current were: 10 A $cm^{-2}$ for part a and 75 A $cm^{-2}$ for part b.

*facing p.* 158

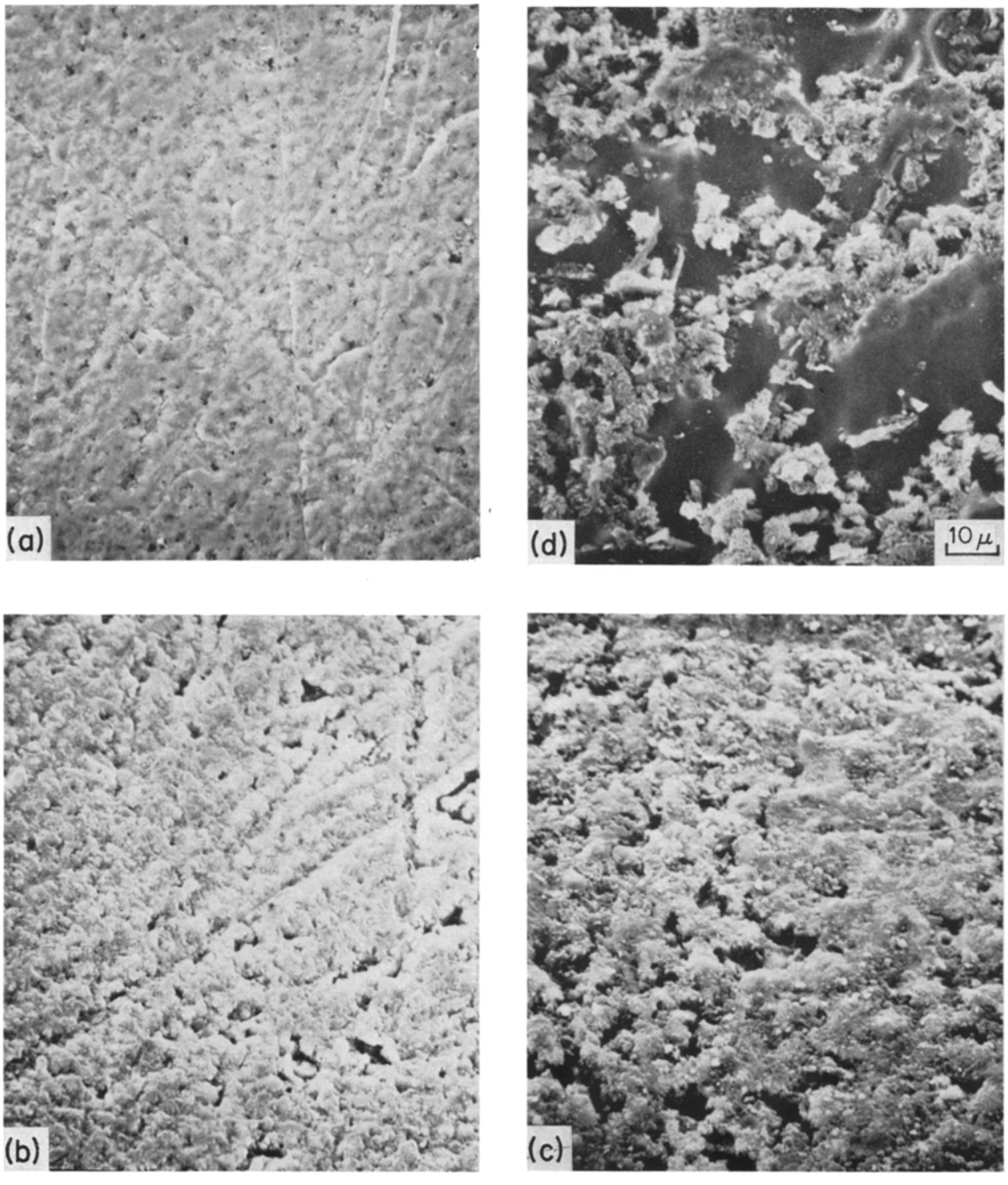


Fig. 6. SEM photomicrographs of mild steel surfaces after dissolution in 4 M $NaNO_3$ at the following current densities: (a) —5 A $cm^{-2}$; (b)—10 A $cm^{-2}$; (c)—50 A $cm^{-2}$; (d)100 A $cm^{-2}$.

*facing p.* 159

current density range agreeing with the current efficiency measurements that the dissolution efficiency was never 100%.

### *3.4 Visual observations*

Optical and scanning electron microscopy were used to examine the mild steel surfaces after dissolution. It was observed that the surface character was directly related to the dissolution current efficiency. At very low current efficiencies, the mild steel surface was covered with a compact black film, and the original polishing lines were clearly visible. As the current efficiency was increased, pits started to appear on the steel surface. With further increase in the current efficiency, the black film became loose and some bare metal surface was exposed to the electrolyte. Finally, at a high current efficiency of 90%, a major portion of the steel became bare; only a small portion was still covered with a loosely adherent film. At this stage, flow lines started to appear on the surface. The film particles were so loose that they could be easily washed away in running water. The film particles were black and differed from the final dissolution product which was brown, colloidal $Fe(OH)_3$.

Fig. 6 is a set of scanning electron microscope (SEM) micrographs of steel surfaces after dissolution in 4 M $NaNO_3$. The experimental conditions for the surfaces shown were: Reynolds number = 17 000; current densities from 5 A $cm^{-2}$ for Fig. 6a to 100 A $cm^{-2}$ for Fig. 6d. Since the SEM requires the samples to be coated with gold, the original black films on the steel appear white on the SEM micrographs. Fig. 6a indicates that at 5 A $cm^{-2}$, the mild steel is covered with a layer of compact film. A careful examination reveals that the small pits in the surface of the film are the initial sites where the intergranular attack takes place. Figs. 6b and 6c show that the pits propagate deeper and wider in the film with increasing current density. Eventually, at 100 A $cm^{-2}$, the film disintegrates completely and a large portion of the metal surface is exposed (Fig. 6d).

## 4. Discussion

Some insight into the anodic process can be gained from a previous mass balance study [5] in which it was found that oxygen is generated during the dissolution of steel in $NaNO_3$ electrolytes at high current densities. Since the oxygen evolution potential of 1·2 V versus SCE is always seen on the open-circuit decay curves (Fig. 5), and since the dissolution efficiency for metal removal never reaches 100%, it is reasonable to assume that two simultaneous reactions are taking place within the current density range investigated. The first reaction is iron dissolution, and the second, oxygen evolution. In the early stage of transpassive dissolution, the current mainly originates in the oxygen evolution reaction. Iron dissolution appears to require the anode potential to pass a certain value, whereupon the rate increases faster than the oxygen reaction rate. This situation is clearly illustrated in Fig. 7 where the IR-free polarization curves reported in Fig. 2 have been separated into two parts: one for iron dissolution and the other for oxygen generation. The apparent current density for iron dissolution is obtained by multiplying the total current density on the polarization curves (Fig. 2) by the current efficiency value reported in Fig. 1. The total current density less the apparent current density for iron dissolution is then used as the apparent

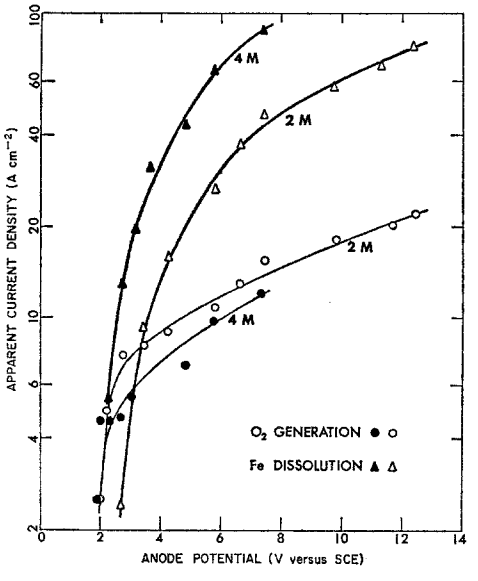


Fig. 7. Apparent current density versus anode potential for the iron dissolution and the oxygen generation reactions in $NaNO_3$ electrolytes.

current density for the oxygen evolution reaction. It is seen that the slope of the iron dissolution curves is greater than that of the oxygen generation curves. Iron dissolution increases in proportion to the nitrate concentration; for a given potential, the apparent dissolution current density in 4 M $NaNO_3$ is about twice that found in 2 M $NaNO_3$. On the other hand, the rate of oxygen evolution appears to decrease with increasing $NaNO_3$ concentration.

Fig. 6 indicates that increase in the current efficiency for the dissolution of mild steel is accompanied by a gradual breakdown of the oxide film on the electrode surface. Such a film is likely composed of an electronically conductive $Fe_3O_4$ matrix [7, 10]. Thus, during the early stage of the transpassive dissolution, the double layer occurs at the film/electrolyte interface, and the current is due to the discharge of adsorbed $H_2O$ molecules resulting in $O_2$ evolution. As the anode potential (or the current density) increases, more and more nitrate ions are adsorbed on the film surface. These ions attack the film and when the current density reaches a threshold value, this becomes so severe that the film starts to break at weak points near the metal grain boundaries. The exact mechanism of the film rupturing process is not known. However, pH of the electrolye has no effect on film breaking, and since the threshold current density increases with decreasing nitrate concentration, one may conclude that adsorption of nitrate ions on the film must be the first step towards the rupture of the oxide film. Once the film is dislocated, the bare metal surface immediately begins to dissolve into the electrolyte causing the current efficiency to increase with increasing current density as shown in Fig. 1. At this point, one may assume that on the anode surface there is exposed metal intermingled with a surface of electronically conductive oxide films. Since the equilibrium potential for iron dissolution is smaller than that for the oxygen evolution reaction, this can only be generated on the areas covered with the oxide film. On the other hand, the rapid iron dissolution can only take place at the metal exposed to the electrolyte. The increase in the current efficiency for iron dissolution with increasing current density is apparently due to a decrease in the filmed surface area. This hypothesis is supported by the current efficiency results and the microscopic observations shown in Figs. 1 and 6. At a low current efficiency, the oxide on the anode is compact, and the high rate iron dissolution can only take place at certain localized areas where the film has broken. At a higher current efficiency, the film particles have been loosened by excessive metal dissolution so that the intermixing of the filmed and unfilmed areas is taking place in a completely random fashion, resulting in uniform dissolution of iron across the anode. The distribution of the surface areas available is a function of current density for a given nitrate concentration upon which the rate of electrolyte flow has no effect, as previously reported [1].

The presence of an oxide film during transpassive dissolution of mild steel in $NaNO_3$ is confirmed by the open-circuit potential decay curves (Fig. 4). Since the first potential arrest on these corresponds to the reduction of $Fe_3O_4$, and the second to the active–passive transition potential, it is reasonable to assume that the length of the plateau is proportional to the amount of oxide film on the anode. The decrease in plateau length with increasing current density is in agreement with the visual observation that the oxide film is loosened and disintegrated with increasing current density or efficiency. At a current density of 1·7 A $cm^{-2}$, 20 s are required after switching off the current, for the electrolyte to penetrate the compact oxide to the underlying metal (curve 4A). However, at 16 A $cm^{-2}$, the film is sufficiently disintegrated that bare metal becomes the dominant feature. Under such conditions, the wave plateau can no longer be observed and the anode potential drops immediately from a high value to the open-circuit equilibrium potential (curve 4E).

Two questions remain to be answered regarding the results reported for which it is difficult to give a reasonable explanation. The first is concerned with the initial 1·6 V (versus SCE) arrest potential on the open-circuit decay curves recorded with a faster time scale on the oscilloscope. The second is the linear relationship between the IR-free potential and the current density. The latter is possibly due to an IR drop across a surface layer on the anodes which

apparently, is beyond the compensation capability of the present current interruption technique. Since the oxide film, adsorbed anions and adsorbed oxygen can all give rise to the IR drop at high current densities, the nature of this layer is unknown.

## 5. Conclusions

We may conclude that two reaction stages take place during the transpassive dissolution of mild steel in sodium nitrate solutions within the current density range investigated. In the early stage the mild steel is covered with a compact layer of an electronically conductive oxide film, and the current is consumed mainly in the generation of oxygen at the film/electrolyte interface. In the second stage, the current density is higher, and the oxide film ruptured by intergranular attack caused by the adsorbed anions on the film surface. Once the film is dislocated, the underlying bare metal surface exposed to the electrolyte begins to dissolve at a high rate, causing an increase in the dissolution current efficiency. The critical current density at which the film starts to break down is found to decrease with increasing nitrate concentrations.

## Acknowledgment

The authors wish to thank Mr D. W. Hardesty, Electrochemistry Department, General Motors Research Laboratories, for his help in the investigation of grain boundaries.

## References

[1] D-T. Chin and A. J. Wallace, *J. Electrochem. Soc.*, **120** (1973) 1487.
[2] D. Landolt, *J. Electrochem. Soc.*, **119** (1972) 708.
[3] D. Landolt, R. H. Muller and C. W. Tobias, in *Fundamentals of Electrochemical Machining*, pp. 200–26, Ed. C. L. Faust, The Electrochemical Society, Inc., Princeton, New Jersey (1971).
[4] D-T. Chin, *J. Electrochem. Soc.*, **119** (1972) 1181.
[5] K-W. Mao, *J. Electrochem. Soc.*, **118** (1971) 1876.
[6] K-W. Mao, *J. Electrochem. Soc.*, **120** (1973) 1056.
[7] K. J. Vetter, *Electrochemical Kinetics*, Academic Press, New York (1967).
[8] G. J. Janz, B. G. Oliver, G. R. Lakshminaryanan and G. E. Mayer, *J. Phys. Chem.*, **74** (1970) 1285.
[9] A. M. Sukhotin and K. M. Kartashova, *Corrosion Sci.*, **5** (1965) 393.
[10] K-W. Mao, M. A. LaBoda and J. P. Hoare, *J. Electrochem. Soc.*, **119** (1972) 419.